Chemical Science

ROYAL SOCIETY OF CHEMISTRY

EDGE ARTICLE

View Article Online
View Journal | View Issue

Cite this: *Chem. Sci.*, 2021, **12**, 11427

All publication charges for this article have been paid for by the Royal Society of Chemistry

Received 16th April 2021
Accepted 20th July 2021

DOI: 10.1039/d1sc02138a

rsc.li/chemical-science

Ruthenium(II)-catalyzed regioselective direct C4- and C5-diamidation of indoles and mechanistic studies†

Shreedhar Devkota, [a] Suyeon Kim, [bc] Seok Yeol Yoo, [bc] Sonaimuthu Mohandoss, [a] Mu-Hyun Baik *[cb] and Yong Rok Lee *[a]

A ruthenium(II)-catalyzed regioselective direct diamidation of 3-carbonylindoles at the C4- and C5-positions using various dioxazolones is described. This novel protocol allows for the effective installation of two amide groups on the benzene ring in indole. A remarkably broad substrate scope, excellent functional group tolerance, and mild reaction conditions are notable features of this protocol. Further explorations reveal that benzo[*b*]thiophene-3-carboxaldehyde is a viable substrate and affords its corresponding diamidation products. The diamido indoles are further converted into various functionalized products and used as sensors for metal ion detection. Density functional theory studies are also conducted to propose a reaction mechanism and provide a detailed understanding of the regioselectivity observed in the reaction.

Introduction

Indoles and their derivatives are among the most important heteroaromatic skeletons found in a wide range of bioactive natural products,[1] functional materials,[2] and pharmaceuticals.[3] They possess a wide range of pharmacological properties, such as antifungal, antihistaminic, antimicrobial, antioxidant, anti-convulsant, anti-HIV, analgesic, anti-inflammatory, anti-cancer, and antitubercular activity.[4] Several substituted indoles are currently utilized as pharmaceuticals.[5] Various synthetic approaches to the preparation of substituted indoles have been demonstrated owing to their importance and useful applications.[6] C3–H functionalization of indoles has been achieved using electrophilic substitution reactions,[7] but functionalization at the C2- and C4-positions remains underdeveloped owing to the inherently poor reactivity at these positions. Recently, significant progress has been made using transition metal-catalyzed C–H functionalization of indoles at the C2- and C4-positions utilizing directing groups.[8] Specifically, the use of carbonyl groups at the C3-site as a directing group for C2–H and C4–H functionalization was demonstrated.[9] Ru(II)- or Rh(III)-catalyzed regioselective C2- and C4-alkenylation or alkylation of 3-carbonylindoles was reported by the Prabhu,[10] Punniyamurthy,[11] and Jia groups.[12] Regioselective Pd-catalyzed direct arylation of 3-carbonylindoles at the C4- or C5-position was reported by the Shi group.[13] For C2- and C4-amination, Ir(III) was shown to be effective and regioselective. C4-Amination of 3-carbonylindoles using sulfonyl azides was described by the Prabhu[14] and You groups[15] (Scheme 1A). Recently, Wang *et al.* developed

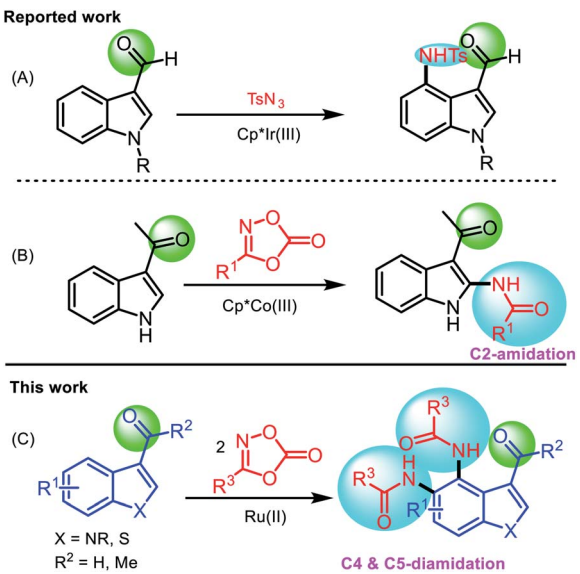

Scheme 1 Reported methods (A and B) *vs.* present strategy (C) for direct amination/amidation of 3-carbonylindoles.

[a]*School of Chemical Engineering, Yeungnam University, Gyeongsan 38541, Republic of Korea. E-mail: yrlee@yu.ac.kr*

[b]*Department of Chemistry, Korea Advanced Institute of Technology (KAIST), Daejeon 34141, Republic of Korea. E-mail: mbaik2805@kaist.ac.kr*

[c]*Center for Catalytic Hydrocarbon Functionalizations, Institute for Basic Science (IBS), Daejeon 34141, Republic of Korea*

† Electronic supplementary information (ESI) available: Experimental procedures, characterization data and X-ray crystallographic structure data for **5i**. CCDC 2070102. For ESI and crystallographic data in CIF or other electronic format see DOI: 10.1039/d1sc02138a

a Co(III)-catalyzed regioselective C2-amidation of 3-acetylindoles using phenyl dioxazolone[16] (Scheme 1B).

To date, diamidation at both the C4- and C5-positions of indole has not been achieved. Recently, dioxazolones have been increasingly recognized as a versatile class of reagents that serve as an amide source, and are environmentally benign, cheap, readily available, and easy to handle.[17] Furthermore, dioxazolones display a potentially useful affinity toward the metal center of metallacyclic intermediates when compared to organic azides, which are considered as conventional amidating reagents.[18] Herein, we report a novel Ru(II)-catalyzed direct diamidation of 3-carbonylindoles using dioxazolones to introduce two amide groups at the C4- and C5-positions of indole (Scheme 1C).

Results and discussion

We first examined the reaction of 1-methylindole-3-carboxaldehyde (**1a**) with 3-phenyl-1,2,4-dioxazol-5-one (**2a**) using various catalysts, additives, and solvents (Table 1). Initial attempts to react **1a** (0.5 mmol) with **2a** (0.5 mmol) in the presence of 5 mol% $[RhCp^*Cl_2]_2$, 15 mol% $AgSbF_6$, and 10 mol% AcOH in 2,2,2-trifluoroethanol (TFE) at 50 °C did not afford the desired product (entry 1, Table 1). When **1a** (0.5 mmol) and **2a** (0.5 mmol) were reacted in the presence of 5 mol% $[Ru(p\text{-cymene})Cl_2]_2$, 15 mol% $AgSbF_6$, and 10 mol% AcOH in TFE at 50 °C for 20 h, diamidation product **5a** was obtained in 40% yield (entry 2). Importantly, the putative products of C2– and C4–H functionalization (**3a** and **4a**) were not observed, indicating the intriguing and useful regioselectivity of the reaction. To our delight, the use of 1.1 mmol of **2a** increased the yield of **5a** to 71% (entry 3). As an alternative to AcOH, the use of 10 mol% 1-$AdCO_2H$, $PhCO_2H$, and PivOH afforded **5a** in 75, 70, and 87% yield, respectively (entries 4–6). The yield of **5a** was not improved by decreasing or increasing the amount of $AgSbF_6$ or PivOH (entries 7–10). In other solvents, such as 1,2-dichloroethane or hexafluoroisopropanol (HFIP), compound **5a** was produced in lower yield (entries 11–12). Increasing the temperature to 70 °C and carrying out the reaction under a N_2 atmosphere did not increase the product yield (entries 13–14). The use of other catalysts did not improve the yield of **5a**. For example, **5a** was isolated in 51% yield when $[Cp^*IrCl_2]_2$ was used as the catalyst, but no **5a** was obtained

Table 1 Optimization of the synthesis of **5a**[a]

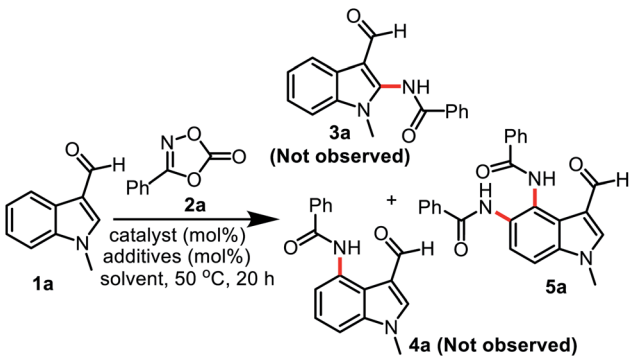

Entry	Catalyst (mol%)	Additives (mol%)	Yield[b] (%) Solvent	5a
1[c]	$[Cp^*RhCl_2]_2$ (5)	$AgSbF_6$ (15), AcOH (10)	TFE	0
2[c]	$[Ru(p\text{-cymene})Cl_2]_2$ (5)	$AgSbF_6$ (15), AcOH (10)	TFE	40
3	$[Ru(p\text{-cymene})Cl_2]_2$ (5)	$AgSbF_6$ (15), AcOH (10)	TFE	71
4	$[Ru(p\text{-cymene})Cl_2]_2$ (5)	$AgSbF_6$ (15), 1-AdCOOH (10)	TFE	75
5	$[Ru(p\text{-cymene})Cl_2]_2$ (5)	$AgSbF_6$ (15), PhCOOH (10)	TFE	70
6	**$[Ru(p\text{-cymene})Cl_2]_2$ (5)**	**$AgSbF_6$ (15), PivOH (10)**	**TFE**	**87**
7	$[Ru(p\text{-cymene})Cl_2]_2$ (5)	$AgSbF_6$ (10), PivOH (10)	TFE	77
8	$[Ru(p\text{-cymene})Cl_2]_2$ (5)	$AgSbF_6$ (20), PivOH (10)	TFE	84
9	$[Ru(p\text{-cymene})Cl_2]_2$ (5)	$AgSbF_6$ (15), PivOH (5)	TFE	79
10	$[Ru(p\text{-cymene})Cl_2]_2$ (5)	$AgSbF_6$ (15), PivOH (20)	TFE	84
11	$[Ru(p\text{-cymene})Cl_2]_2$ (5)	$AgSbF_6$ (15), PivOH (10)	1,2-DCE	43
12	$[Ru(p\text{-cymene})Cl_2]_2$ (5)	$AgSbF_6$ (15), PivOH (10)	HFIP	67
13[d]	$[Ru(p\text{-cymene})Cl_2]_2$ (5)	$AgSbF_6$ (15), PivOH (10)	TFE	65
14[e]	$[Ru(p\text{-cymene})Cl_2]_2$ (5)	$AgSbF_6$ (15), PivOH (10)	TFE	75
15	$[Cp^*IrCl_2]_2$ (5)	$AgSbF_6$ (15), PivOH (10)	TFE	51
16	$[Cp^*Co(CO)I_2]$ (5)	$AgSbF_6$ (15), PivOH (10)	TFE	0

[a] Reaction conditions: **1a** (0.5 mmol), **2a** (1.1 mmol), solvent (5 mL), and air atmosphere. [b] Isolated yield. [c] **1a** (0.5 mmol), **2a** (0.5 mmol), and solvent (5 mL). [d] The reaction was performed under a N_2 atmosphere. [e] The reaction was carried out at 70 °C.

Table 2 Substrate scope of indole-3-carboxaldehydes

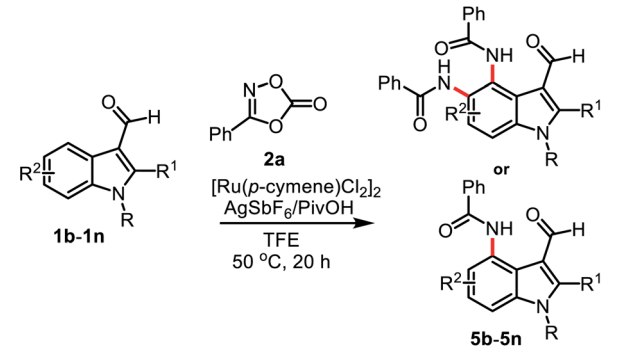

(A) Substrate scope of N–H and *N*-substituted indole-3-aldehydes

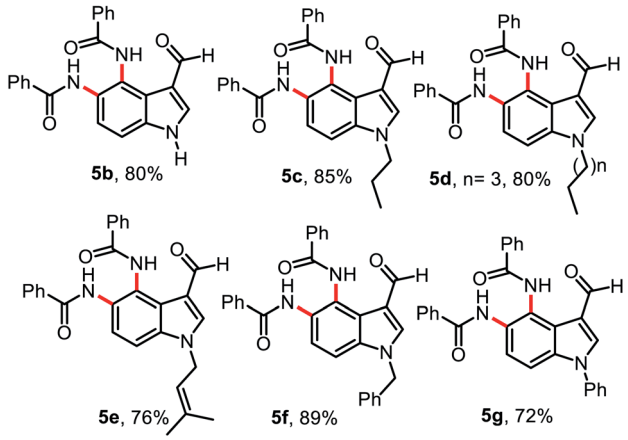

(B) Substrate scope of C2-, C5-, C6-, and C7-substituted indole-3-aldehydes

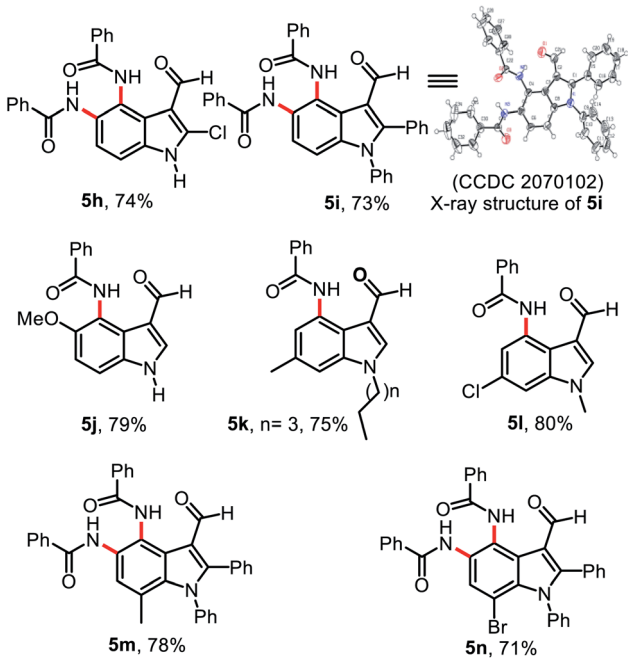

Table 3 Substrate scope of dioxazolones bearing aryl and alkyl groups

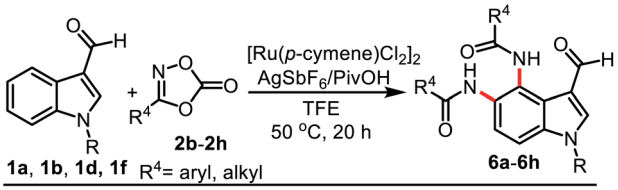

(A) Substrate scope of dioxazolones bearing aryl groups

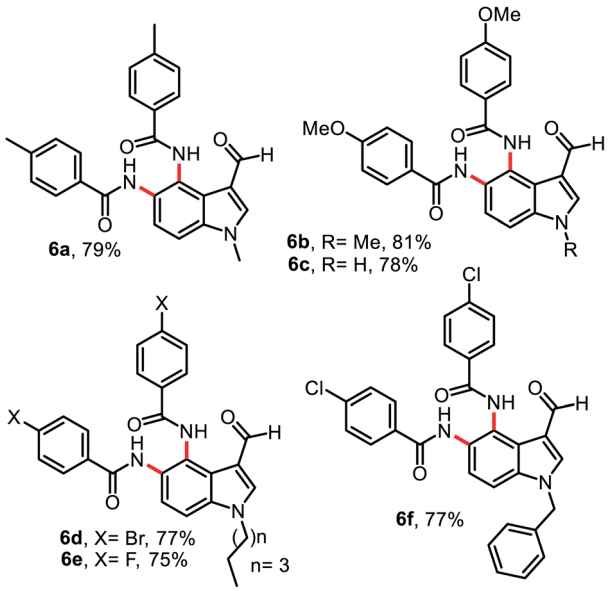

(B) Substrate scope of dioxazolones bearing alkyl groups

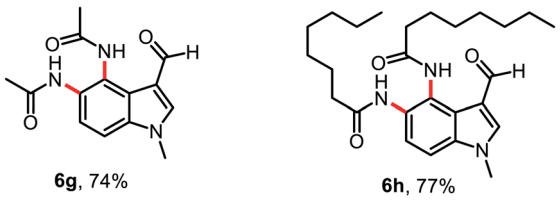

from [Cp*Co(CO)I_2] (entries 15–16). The ^{1}H NMR of **5a** showed a singlet corresponding to the aldehyde proton at δ 9.64 ppm, the vinyl proton on the pyrrole ring at δ 8.42 ppm as a singlet, and two amide proton peaks at δ 11.67 and 9.89 ppm as two singlets. The ^{13}C NMR spectrum showed an aldehyde carbon peak at δ 184.9 ppm and two amide carbon peaks at δ 165.9 and 164.2 ppm, respectively. When an excess of **2a** (4.4 equivalents) was used to introduce amide substituents at C-4, 5, 6, 7 of the indole ring, only **5a** was produced in 86% yield without formation of other products. Further reaction of *N*-methyl-indole with **2a** under standard reaction conditions did not afford the amidation product.

The scope was explored using the optimized conditions employing various indole-3-carboxaldehyde substrates (**1b–1n**) and dioxazolone **2a** (Table 2). Treatment of unsubstituted indole-3-carboxaldehyde **1b** and *N*-alkyl substituted indole-3-carboxaldehydes **1c–1d** bearing *n*-propyl and *n*-pentyl groups provided their corresponding products **5b–5d** in 80, 85, and 80% yield, respectively (Table 2, A). Similarly, treatment of substituted indole-3-carboxaldehydes **1e–1g** bearing *N*-prenyl, *N*-benzyl, and *N*-phenyl groups afforded their corresponding

Table 4 Substrate scope of dioxazolones bearing heteroaromatics, polyaromatic rings, benzo[*b*]thiophene-3-carboxaldehyde, and 3-acylindole

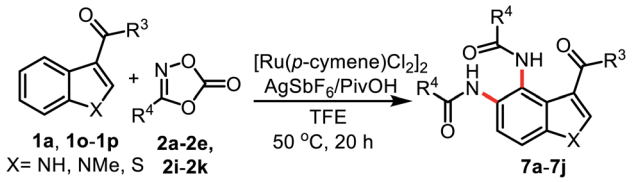

(A) Substrate scope of dioxazolones bearing heteroaromatic and polyaromatic ring

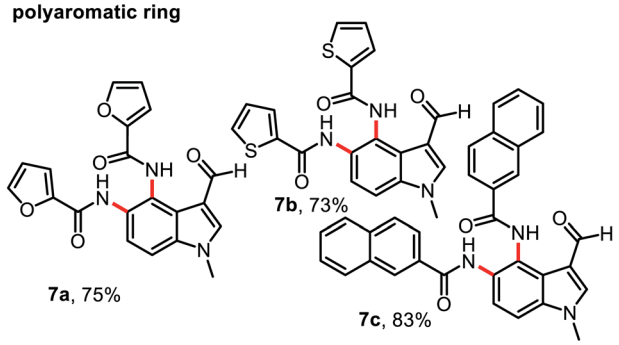

(B) Substrate scope of benzo[*b*]thiophene-3-carboxaldehyde

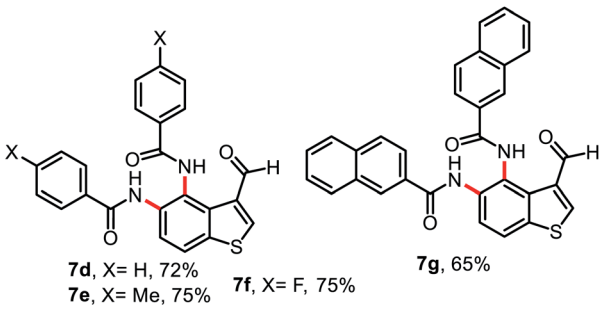

(C) Substrate scope of 3-acylindole

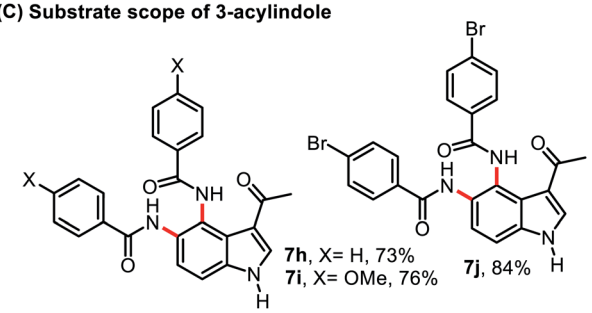

products **5e**–**5g** in 76, 89, and 72% yield, respectively. After exploring the reactions using different *N*-substituted indoles, we then investigated a series of indoles bearing various substituents on the indole ring. C2-Chloro- or C2-phenyl substituted indole-3-carboxaldehydes **1h** and **1i** gave compounds **5h** and **5i** in 74 and 73% yield, respectively (Table 2, B). The structure of **5i** was unambiguously confirmed using single-crystal X-ray diffraction (CCDC 2070102†). Interestingly, when C5- and C6-substituted indole-3-carboxaldehydes **1j**, **1k**, and **1l** were used in the reaction, mono amidation products **5j**–**5l** were isolated in 79, 75 and 80% yield, respectively and their corresponding diamidation products were not produced, which was attributed to the steric bulk of these substituents. In addition, the reaction of C7-substituted indole-3-carboxaldehydes **1m** and **1n** successfully provided their diamidation products **5m** and **5n** in 78 and 71% yield, respectively.

To demonstrate the scope of this protocol, various dioxazolones were examined in the reaction under the optimal conditions (Table 3). A combination of **1a** or **1b** with dioxolones **2b**–**2c** having electron-donating groups of 4-Me or 4-OMe on the aromatic ring showed good reactivity and provided products **6a**–**6c** in 78–81% yield. Similarly, dioxazolones **2d**–**2f** bearing electron-withdrawing groups on the aromatic ring such as 4-Br, 4-F, and 4-Cl were also tolerated in the reaction and provided diamidation products **6d**–**6f** in 75–77% yield (Table 3, A). We found that this reaction was not limited to aryl substrates only; aliphatic dioxazolones **2g** and **2h** bearing methyl and *n*-heptyl groups also displayed a good functional group compatibility, affording products **6g** and **6h** in 74 and 77% yield, respectively (Table 3, B).

We further explored the scope of this reaction using dioxolones **2i**–**2k** bearing heteroaromatic and polyaromatic one (**2j**) which afforded products **7a** and **7b** in 75% and 73% yield. When **1a** was reacted with 3-(naphthalen-2-yl)-1,4,2-dioxazol-5-one (**2k**), the desired product **7c** was isolated in 83% yield (Table

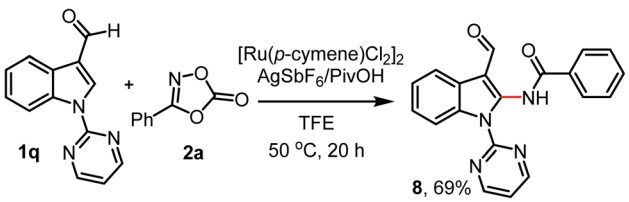

Scheme 2 Reaction of **1q** with **2a**.

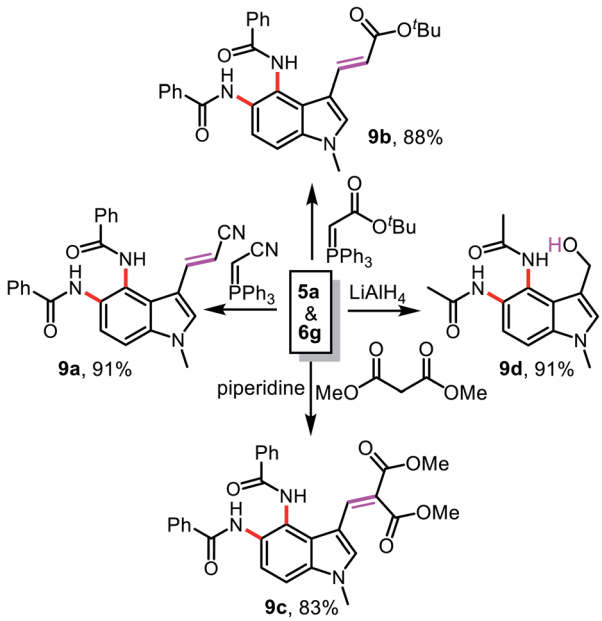

Scheme 3 Further functionalization of compounds **5a** and **6g**.

4, A). To test the versatility of the C–H activation/amidation reaction, which is not restricted to indole-3-formylaldehydes, the possibility of using benzo[*b*]thiophene-3-carboxaldehyde (**1o**) and 3-acylindole (**1p**) was investigated (Table 4, B and C). Gratifyingly, a combination of **1o** with **2a**, **2b**, **2e**, or **2k** successfully gave products **7d**–**7g** in 65–75% yield. The reactions of 3-acylindole **1p** were also successful and provided products **7h**–**7j** in 73–84% yield.

Next, we performed the reaction of **1q** bearing C3-formyl and *N*-pyrimidyl directing groups with **2a** under the standard reaction conditions (Scheme 2). However, instead of C4/C5-diamidation or C7-amidation products, only C2-amidated product **8** was obtained in 69% yield (Scheme 2).

The compounds **5a** and **6g** obtained using this new protocol are useful precursors for further synthetic transformations like Wittig olefination, Knoevenagel condensation, and reduction reactions, as summarized in Scheme 3. Treatment of **5a** with (triphenylphosphoranylidene)acetonitrile or (*t*-butoxycarbonylmethylene)triphenylphosphorane in THF led to **9a** and **9b** in 91 and 88% yield, respectively. The condensation reaction of **5a** with dimethyl malonate in the presence of piperidine afforded compound **9c** in 83% yield. The chemoselective reduction of **6g** using $LiAlH_4$ in THF gave compound **9d** in 91% yield.

To gain insight into the mechanism of this reaction, we performed H/D exchange experiments using **1a** with 5 mol% [Ru(*p*-cymene)Cl_2]$_2$, 15 mol% $AgSbF_6$, and 5 equiv. of CD_3COOD as the deuterium source in TFE at 50 °C. The ^{1}H NMR spectrum of **1a′** showed 11% H/D exchange at the C4-position, while no significant H/D exchange was observed at the C2-position (Scheme 4).

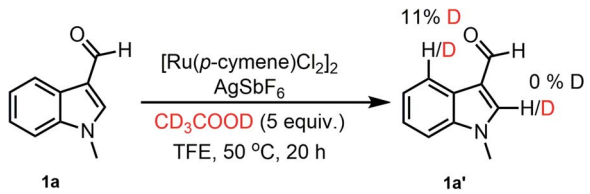

Scheme 4 Control experiment.

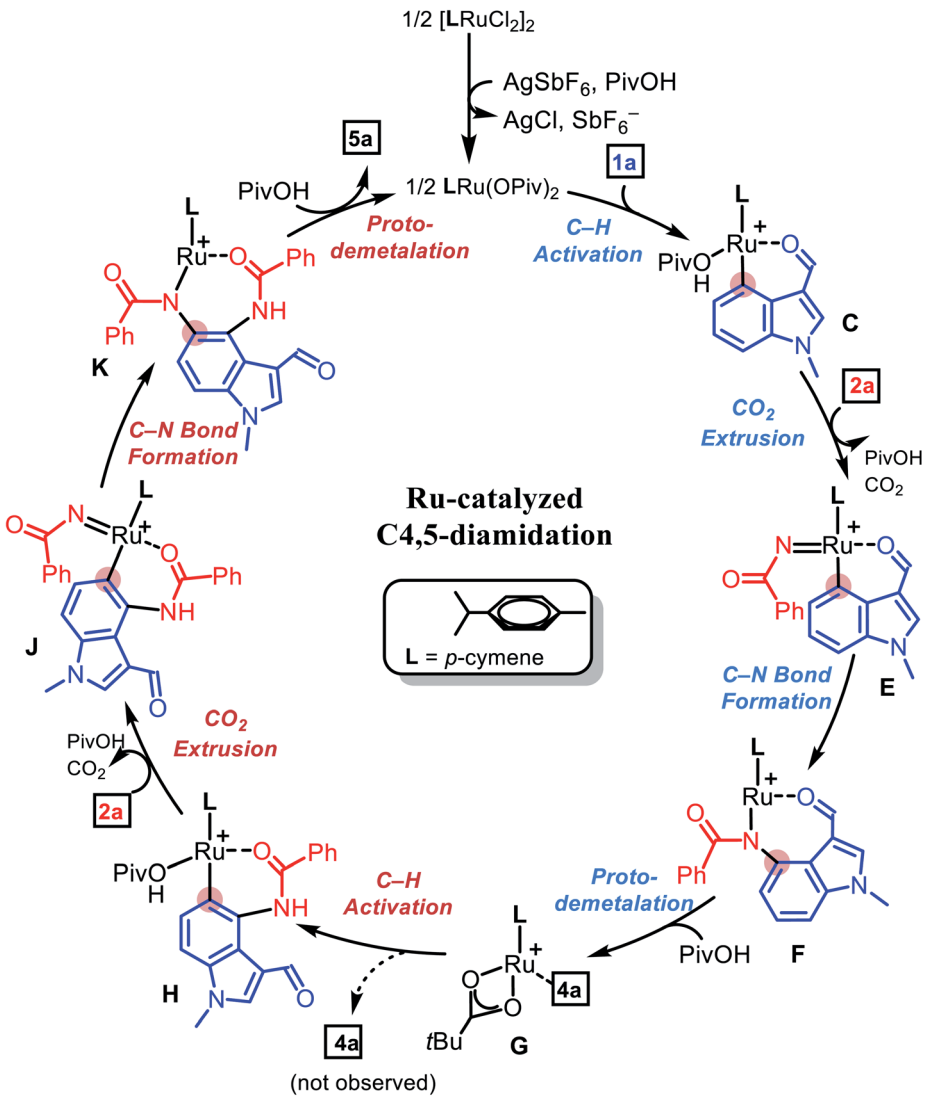

Scheme 5 Plausible mechanism for the formation of **5a**.

Based on our H/D exchange experiments and the observed products, a plausible mechanism for the Ru(II)-catalyzed diamidation of indole was proposed, as shown in Scheme 5, which was explicitly tested using density functional theory (DFT) calculations.[10,12] Geometry optimization, vibration, and solvation energy calculations were performed using the B3LYP-D3/LACVP/6-31G** level of theory.[19] The electronic energies of all the optimized structures were re-evaluated at the B3LYP-D3/cc-pVTZ(-f) level of theory.[20] Details of the computational method can be found in the ESI.† As shown in Fig. 1, our

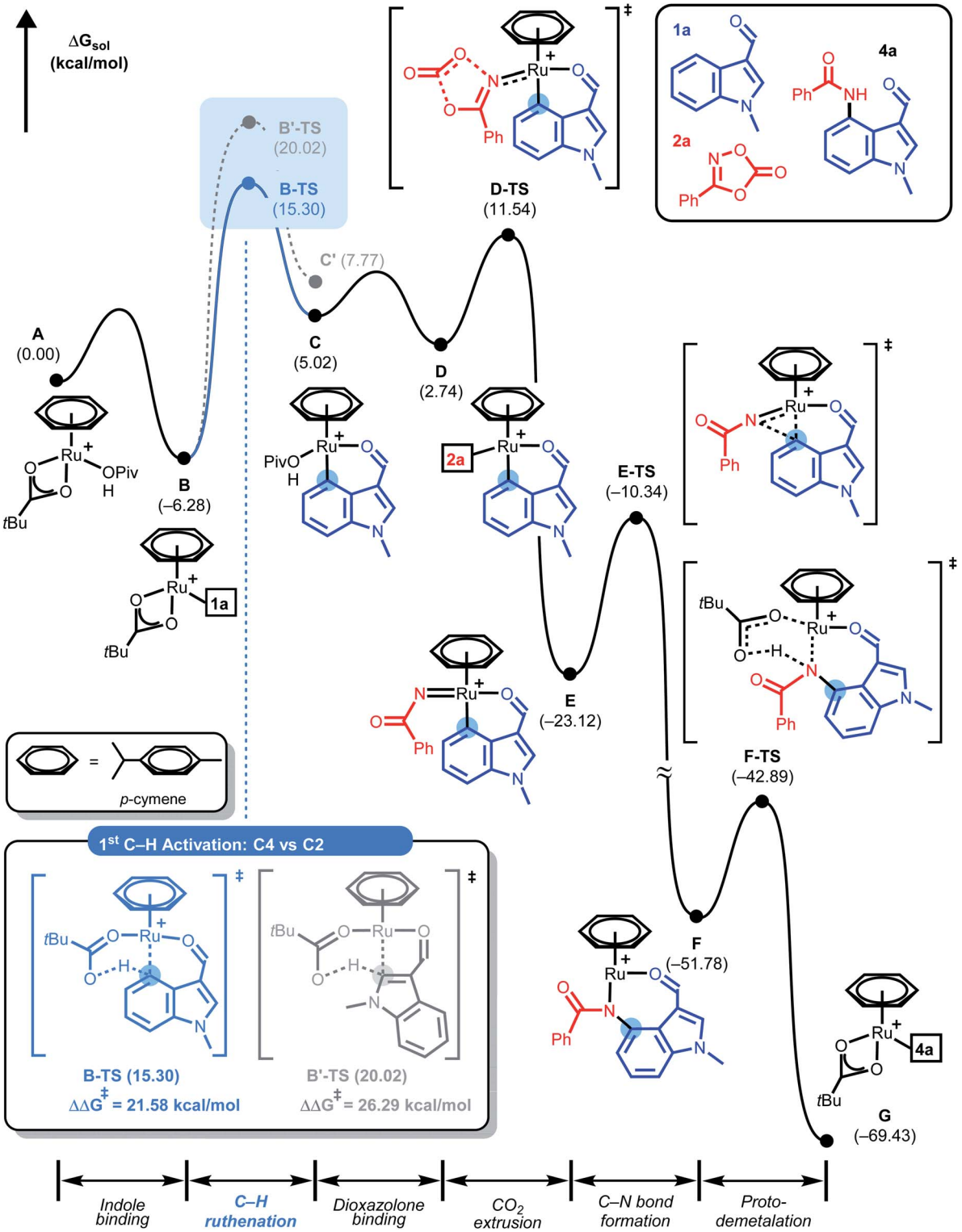

Fig. 1 DFT-calculated energy profile obtained for the Ru(II)-catalyzed C4-amidation reaction of **1a**.

theoretical investigation started with cationic Ru(II) κ^2-OPiv complex **A** as the active catalyst. The dissociation of one neutral ligand allows the metal center to accommodate the indole substrate, 1-methylindole-3-carboxaldehyde (**1a**), to give **B**, which was found to be 6.3 kcal mol^{-1} more stable than the initial species. C4–H ruthenation occurs to form a six-membered ruthenacycle **C** traversing **B-TS** located at 15.3 kcal mol^{-1}. The regioisomeric transition state (**B′-TS**) for C2–H activation demands an additional energy of 4.7 kcal mol^{-1}, indicating a significant kinetic preference for C4-functionalization over C2.

To gain a deeper understanding of the C–H ruthenation step that governs the regioselectivity of the first amidation reaction, the energy difference between **B-TS** and **B′-TS** was examined using distortion–interaction analysis.[21] Fig. 2 shows that the complex was partitioned into the indole substrate and catalyst fragments to obtain the structural distortion energies (E_{dist}) required for each fragment to adopt the structure observed in the transition state. The interaction energy (E_{int}) was calculated by letting the two distorted fragments interact electronically at the distance observed in the transition state. Substrate **1a** exhibits a slightly larger destabilization energy of ~1 kcal mol^{-1} for the elongation of C4–H when compared to C2–H despite having almost identical bond lengths of 1.228 and 1.227 Å, respectively, reflecting the lower acidity of C4–H.

Because the catalyst distortions are also nearly identical at ~31.5 kcal mol^{-1}, the total distortion energies can be considered nearly identical at 56.0 and 55.2 to give an overall electronic energy preference of 3.2 kcal mol^{-1}. Interestingly, the interaction energies show a significant difference with the E_{int} in the transition states being 4 kcal mol^{-1}, as illustrated in Fig. 2. As the main electronic interactions in these two transition states are related to the Ru–C and O–H bond forming steps, the difference in E_{int} likely reflects the reactivity at the carbon sites in **1a**. Thus, the electronic properties of each carbon site in **1a** were evaluated using natural population analysis (NPA) and the Fukui index, indicating that the C4-site was more electron-rich than the C2-site (Fig. S1, see ESI†). This analysis indicates that the relative energies of the two possible transition states were governed by the higher partial negative charge on the C4-site, which leads to a stronger interaction with the electrophilic metal site. This is an unexpected result because the kinetics of conventional concerted metalation–deprotonation (CMD) reactions are thought to be mainly determined by the Brønsted acidity of the C–H bonds. Thus C–H activation in this system is best described as an electrophilic CMD (eCMD), which was recently highlighted as an alternative to the classical CMD mechanism.[22] The C4–H activation step affords six-membered ruthenacycle **C**, which was 2.8 kcal mol^{-1} lower in energy than the alternative five-membered ruthenacycle (**C′**).

To push the catalytic cycle forward, the PivOH ligand in **C** must be displaced by 3-phenyl-1,2,4-dioxazol-5-one (**2a**) to form *N*-bound complex **D** located at 2.7 kcal mol^{-1}. CO_2 extrusion *via* **D-TS** at 11.5 kcal mol^{-1} forms *N*-bound complex **D** located at 2.7 kcal mol^{-1}. CO_2 extrusion *via* **D-TS** at 11.5 kcal mol^{-1} presented Ru(IV) imido complex **E**, which can undergo a reductive C–N bond forming reaction. Traversing reductive elimination

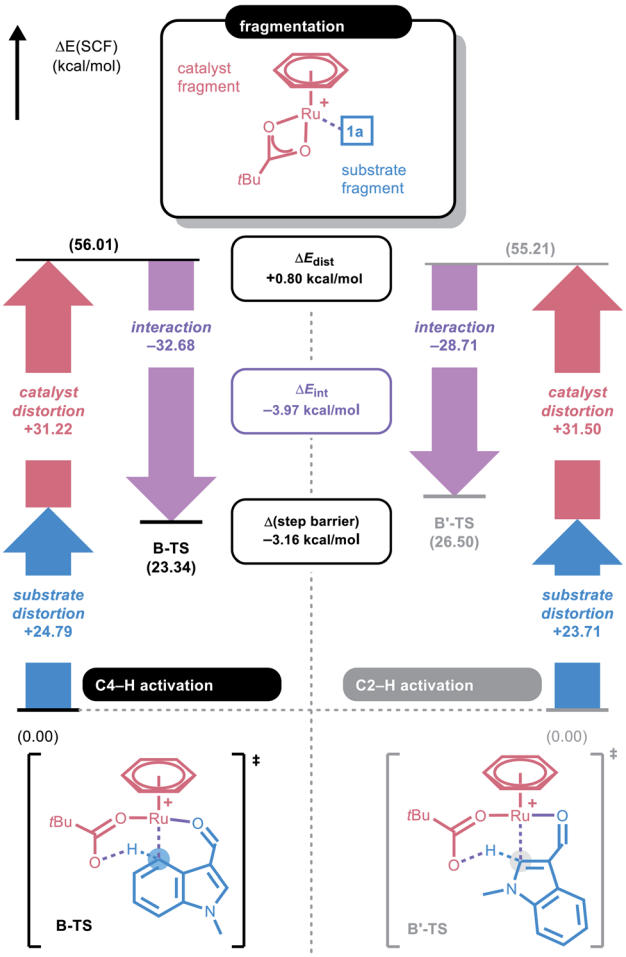

Fig. 2 Distortion–interaction analysis diagram for B-TS and B′-TS.

transition state **E-TS** demands 12.8 kcal mol^{-1}, which generates cyclic amidato complex **F** at −51.8 kcal mol^{-1}. To complete the first amidation reaction proto-demetallation occurs with the assistance of PivOH to regenerate the κ^2-OPiv moiety in **G** for the sequential C–H activation of **4a**. In principle, mono-amidated indole product **4a** may be released from **G**, but for diamidation to occur, **4a** may remain coordinated to the ruthenium center, in line with the experimental observation that **4a** was not detected. As summarized in Fig. 3, our calculations show that C5–H ruthenation enhanced reactivity was attributed to the electron-donating and resonance effects of the C4-amide group, which increase the electron density and nucleophilicity of the C5-site. The potential competing C2–H activation of **4a** was evaluated and discarded as it requires an insurmountable barrier of 32.0 kcal mol^{-1} associated with **G′-TS**. Distortion–interaction analysis revealed that the difference in E_{int} between **G-TS** and **G′-TS** was 20.1 kcal mol^{-1}, which was greater than that found in the first C–H activation step (Fig. S2, see ESI†). Consumption of another equivalent of **2a** and CO_2 extrusion traversing **I-TS** located at 18.6 kcal mol^{-1} gave imido ruthenacycle **J**. Subsequent C–N bond formation and proto-demetallation regenerate the active catalyst (**A**) and furnish the desired diamidated product **5a**. In principle, C5-amidation may facilitate C6–H activation in a similar way; the increased

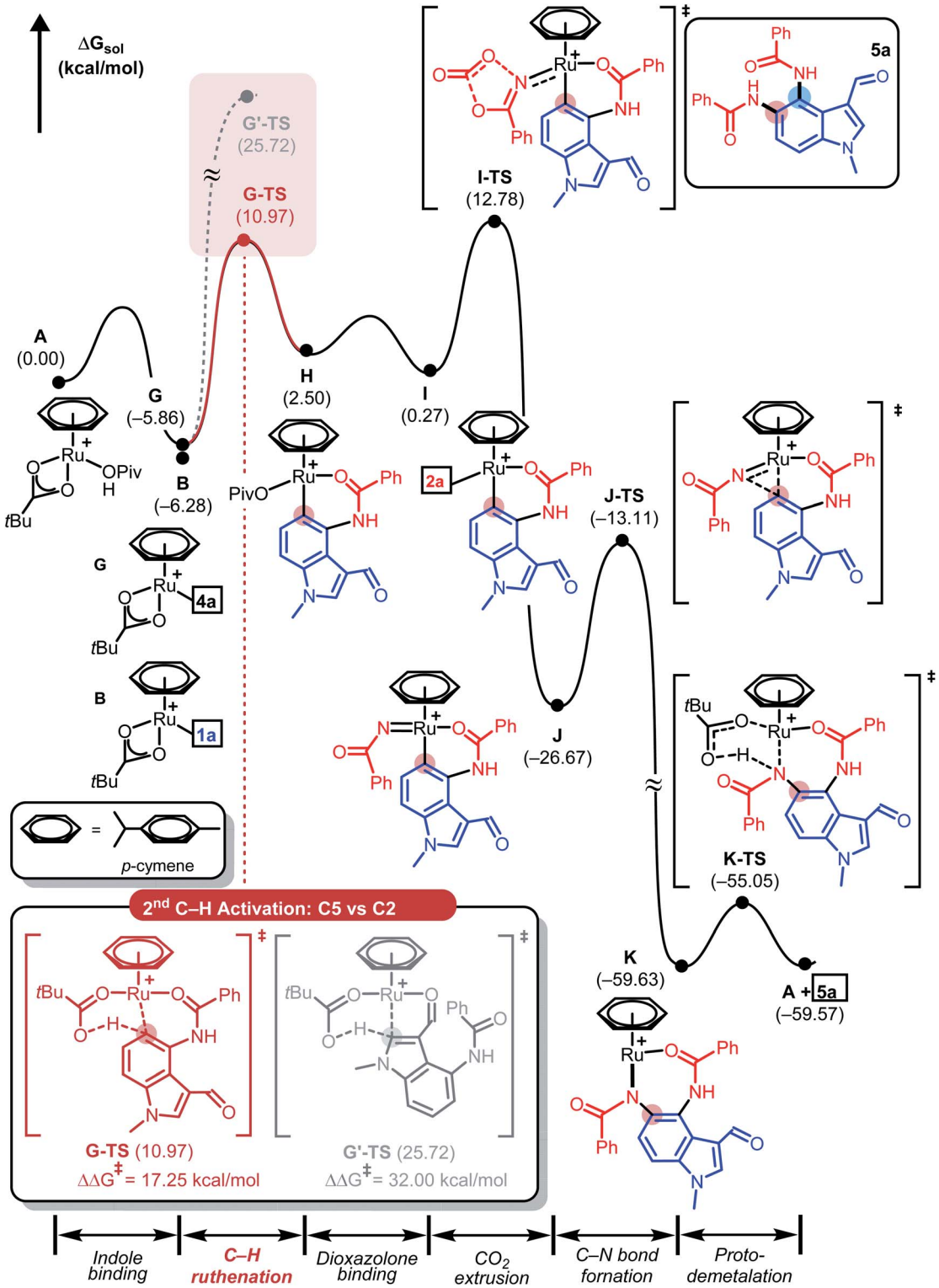

Fig. 3 DFT-calculated energy profile for the consecutive Ru(II)-catalysed C5-amidation reaction used to give **5a**.

structural complexity and steric bulk destabilize the resulting ruthenacycle intermediates and further impede the reaction (Fig. S3, see ESI†).[23]

Indole-based receptor systems have attracted significant attention because of the inherent fluorescence properties of indole chromophores.[24] The indole fluorophore can transfer an electron to the vacant orbital in transition metals. In addition, the interaction between the indole ring and metal in biological systems has been well documented.[25] However, indole derivatives used as potential fluorescent chemosensors for sensing

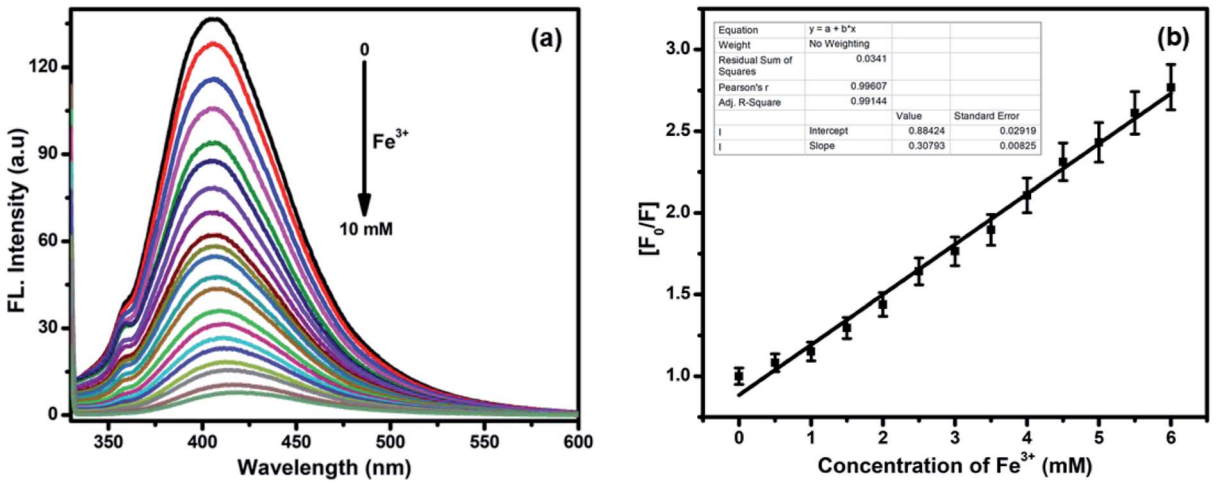

Fig. 4 (a) Fluorescence spectra of **7i** (1.0×10^{-5} mol L^{-1}) in the presence of various concentrations of Fe^{3+} (0–10 mM). (b) Stern–Volmer plot based on the relative fluorescence signal [F_0/F] and [Fe^{3+}] concentrations.

metal cations such as ferric ions (Fe^{3+}) have been less explored.[26] Iron is the most abundant element on the Earth and in living cells. Iron is essential for cellular metabolism, enzymatic reactions, and gene expression, and serves as an oxygen carrier in hemoglobin.[27] Deficiency or excess Fe^{3+} in biological systems can cause various disorders. Therefore, the detection, sensing, and monitoring of Fe^{3+} ions have become a matter of significant concern in environmental and biological samples.

The fluorescence intensities of compounds **5a–5o**, **6a–6h**, and **7a–7j** were examined. These compounds exhibit fluorescence due to the presence of NH groups and other active sites, which can be used to selectively detect and bind to heavy metal ions (Fig. S4, see ESI†). Interestingly, among the screened compounds, **7i** showed the most intense fluorescence signal (Fig. S5, see ESI†). Fig. S6† shows the absorbance and fluorescence selectivity response of compound **7i** (1.0×10^{-5} mol L^{-1}) dissolved in DMSO towards 10 mM pH 7.4 solutions of different metal ions such as Ag^{+}, Ba^{2+}, Ca^{2+}, Cd^{2+}, Ce^{3+}, Cu^{2+}, Co^{2+}, Fe^{3+}, Hg^{2+}, Mn^{2+}, Na^{+}, Ni^{2+}, Pb^{2+}, Sn^{2+}, Sr^{2+}, Ti^{3+}, and Zn^{2+}. Fig. S6a (see the ESI†) shows that **7i** exhibits maximum absorption bands at 306, 294, and 330 nm upon the addition of Ce^{3+}, Cu^{2+}, and Fe^{3+} ions, respectively. The presence of Ce^{3+}, Cu^{2+}, and Fe^{3+} ions results in a shift and enhancement of the absorption intensity of **7i**, while the response of **7i** towards other metal ions was negligible.[28] Among the metal ions studied, Fe^{3+} ions show a maximum tendency to quench the fluorescence intensity of **7i** due to the formation of a **7i**–Fe^{3+} complex (Fig. S6b, see ESI†). Upon the addition of Fe^{3+} (0 to 10 mM), the emission intensity of **7i** gradually decreases, accompanied by a red shift of 12 nm from 405 nm to 417 nm, up on excitation at 324 nm (Fig. 4a). The binding of Fe^{3+} to **7i** initiates charge transfer causing 95% fluorescence quenching.[29] According to the linear Stern–Volmer equation, the measured fluorescence intensity [F_0/F] varied as a function of the concentration of Fe^{3+}, which showed good linearity, confirming the formation of **7i**–Fe^{3+} (Fig. 4b). Based on our fluorescence titration experiments, the detection limit of **7i**–Fe^{3+} was found to be 2.9 μM (Fig. S7, see ESI†).[30]

Conclusions

In conclusion, we have developed a new method to introduce two amide groups at the C4- and C5-positions of indole using a ruthenium(II)-catalyzed regioselective diamidation of 3-carbonylindoles with various dioxazolones. This novel diamidation protocol effectively provides access to a diverse series of functionalized indoles carrying two amide groups on the benzene ring of the indole moiety under mild conditions with excellent functional group tolerance and a broad substrate scope. Density functional theory calculations elucidated the full reaction mechanism and rationalized the regioselectivity observed in the reaction. Further extension of this protocol can also afford the corresponding diamidation products using benzo[*b*]thiophene-3-carboxaldehyde. To demonstrate the utility of this new method, the synthesized compounds were further elaborated and converted into functionalized molecules, which can be used as sensors for metal ion detection.

Data availability

The datasets supporting this article have been uploaded as part of the ESI.†

Author contributions

S. D. performed all the experiments and prepared the ESI.† S. K., S. Y. Y. and M.-H. B. carried out all the computational studies. S. M. performed the chemosensor studies. Y. R. L. conceptualized the work, supervised the project and wrote the manuscript. All the authors discussed and commented to give the final shape of the manuscript.

Conflicts of interest

There are no conflicts to declare.

Acknowledgements

This work was supported by the National Research Foundation of Korea (NRF) grant funded by the Korean government (MSIT) (2021R1A2B5B02002436) and by the Korean Ministry of Education, Science, and Technology (2012M3A7B4049677). We also thank the Institute for Basic Science (IBS-R10-A1) for their financial support.

Notes and references

1 (*a*) M. Inman and C. J. Moody, *Chem. Sci.*, 2013, **4**, 29–41; (*b*) A. J. Kochanowska-Karamyan and M. T. Hamann, *Chem. Rev.*, 2010, **110**, 4489–4497; (*c*) M. Ishikura, T. Abe, T. Choshi and S. Hibino, *Nat. Prod. Rep.*, 2013, **30**, 694–752; (*d*) T. Kawasaki and K. Huguchi, *Nat. Prod. Rep.*, 2005, **22**, 761–793.

2 (*a*) Y. Liu, K. Ai and L. Lu, *Chem. Rev.*, 2014, **114**, 5057–5115; (*b*) C. W. Lee and J. Y. Lee, *Adv. Mater.*, 2013, **25**, 5450–5454.

3 (*a*) T. V. Sravanthi and S. L. Manju, *Eur. J. Pharm. Sci.*, 2016, **91**, 1–10; (*b*) A. Kumari and R. K. Singh, *Bioorg. Chem.*, 2019, **89**, 103021–103056.

4 (*a*) N. Chadha and O. Silakari, *Eur. J. Med. Chem.*, 2017, **134**, 159–184; (*b*) N. K. Kaushik, N. Kaushik, P. Attri, N. Kumar, C. H. Kim, A. K. Verma and E. H. Choi, *Molecules*, 2013, **18**, 6620–6662; (*c*) P. V. Thanikachalam, R. K. Maurya, V. Garg and V. Monga, *Eur. J. Med. Chem.*, 2019, **180**, 562–612.

5 R. D. Taylor, M. MacCoss and A. D. G. Lawson, *J. Med. Chem.*, 2014, **57**, 5845–5859.

6 (*a*) Z. Wang, H. Zeng and C.-J. Li, *Org. Lett.*, 2019, **21**, 2302–2306; (*b*) S. G. Newman and M. Lautens, *J. Am. Chem. Soc.*, 2010, **132**, 11416–11417; (*c*) N. Selander, B. T. Worrell, S. Chuprakov, S. Velaparthi and V. V. Fokin, *J. Am. Chem. Soc.*, 2012, **134**, 14670–14673; (*d*) S. Wagaw, B. H. Yang and S. L. Buchwald, *J. Am. Chem. Soc.*, 1998, **120**, 6621–6622.

7 (*a*) S. Chen, Y. Liao, F. Zhao, H. Qi, S. Liu and G.-J. Deng, *Org. Lett.*, 2014, **16**, 1618–1621; (*b*) J. Chen, M. Li, J. Zhang, W. Sun and Y. Jiang, *Org. Lett.*, 2020, **22**, 3033–3038; (*c*) G. Berionni, V. Morozova, M. Heininger, P. Mayer, P. Knochel and H. Mayr, *J. Am. Chem. Soc.*, 2013, **135**, 6317–6324.

8 (*a*) R. Mei, J. Loup and L. Ackermann, *ACS Catal.*, 2016, **6**, 793–797; (*b*) Z. Ding and N. Yoshikai, *Angew. Chem., Int. Ed.*, 2012, **51**, 4698–4701; (*c*) Q. Liu, Q. Li, Y. Ma and Y. Jia, *Org. Lett.*, 2013, **15**, 4528–4531.

9 (*a*) M. S. Sherikar, R. Kapanaiah, V. Lanke and K. R. Prabhu, *Chem. Commun.*, 2018, **54**, 11200–11203; (*b*) A. J. Borah and Z. Shi, *Chem. Commun.*, 2017, **53**, 3945–3948; (*c*) F. Li, Y. Zhou, H. Yang, Z. Wang, Q. Yu and F.-L. Zhang, *Org. Lett.*, 2019, **21**, 3692–3995.

10 (*a*) V. Lanke, K. R. Bettadapur and K. R. Prabhu, *Org. Lett.*, 2016, **18**, 5496–5499; (*b*) V. Lanke and K. R. Prabhu, *Org. Lett.*, 2013, **15**, 6262–6265.

11 S. Pradhan, M. Mishra, P. B. De, S. Banerjee and T. Punniyamurthy, *Org. Lett.*, 2020, **22**, 1720–1725.

12 J. Lv, B. Wang, K. Yuan, Y. Wang and Y. Jia, *Org. Lett.*, 2017, **19**, 3664–3667.

13 Y. Yang, P. Gao, Y. Zhao and Z. Shi, *Angew. Chem., Int. Ed.*, 2017, **56**, 3966–3971.

14 V. Lanke and K. R. Prabhu, *Chem. Commun.*, 2017, **53**, 5117–5120.

15 S. Chen, B. Feng, X. Zheng, J. Yin, S. Yang and J. You, *Org. Lett.*, 2017, **19**, 2502–2505.

16 X. Shi, W. Xu, R. Wang, X. Zeng, H. Qiu and M. Wang, *J. Org. Chem.*, 2020, **85**, 3911–3920.

17 (*a*) J. Park and S. Chang, *Angew. Chem., Int. Ed.*, 2015, **54**, 14103–14107; (*b*) S. Fukagawa, Y. Kato, R. Tanaka, M. Kojima, T. Yoshino and S. Matsunaga, *Angew. Chem., Int. Ed.*, 2019, **58**, 1153–1157; (*c*) B. Sun, T. Yoshino, S. Matsunaga and M. A. Kanai, *Chem. Commun.*, 2015, **51**, 4659–4661; (*d*) P. W. Tan, A. M. Mak, M. B. Sullivan, D. J. Dixon and J. Seayad, *Angew. Chem., Int. Ed.*, 2017, **56**, 16550–16554.

18 Y. Park, J. Heo, M.-H. Baik and S. Chang, *J. Am. Chem. Soc.*, 2016, **138**, 14020–14029.

19 (*a*) J. C. Slater, *Phys. Today*, 1974, **27**, 49; (*b*) A. D. Becke, *Phys. Rev. A: At., Mol., Opt. Phys.*, 1988, **38**, 3098–3100; (*c*) C. Lee, W. Yang and R. G. Parr, *Phys. Rev. B: Condens. Matter Mater. Phys.*, 1988, **37**, 785–789; (*d*) A. D. Becke, *J. Chem. Phys.*, 1993, **98**, 5648–5652; (*e*) S. Grimme, J. Antony, S. Ehrlich and S. Krieg, *J. Chem. Phys.*, 2010, **132**, 154104; (*f*) W. J. Hehre, R. Ditchfield and J. A. Pople, *J. Chem. Phys.*, 1972, **56**, 2257–2261; (*g*) P. J. Hay and W. R. Wadt, *J. Chem. Phys.*, 1985, **82**, 270–283; (*h*) W. R. Wadt and P. J. Hay, *J. Chem. Phys.*, 1985, **82**, 284–298; (*i*) P. J. Hay and W. R. Wadt, *J. Chem. Phys.*, 1985, **82**, 299–310.

20 T. H. Dunning, *J. Chem. Phys.*, 1989, **90**, 1007–1023.

21 F. M. Bickelhaupt and K. N. Houk, *Angew. Chem., Int. Ed.*, 2017, **56**, 10070–10086.

22 (*a*) L. Wang and B. P. Carrow, *ACS Catal.*, 2019, **9**, 6821–6836; (*b*) E. Tan, O. Quinonero, M. E. de Orbe and A. M. Echavarren, *ACS Catal.*, 2018, **8**, 2166–2172; (*c*) K. Naksomboon, J. Poater, F. M. Bickelhaupt and M. Á. Fernández-Ibáñez, *J. Am. Chem. Soc.*, 2019, **141**, 6719–6725; (*d*) D. Zell, M. Bursch, V. Müller, S. Grimme and L. Ackermann, *Angew. Chem., Int. Ed.*, 2017, **56**, 10378–10382; (*e*) T. Rogge, J. C. A. Oliveira, R. Kuniyil, L. Hu and L. Ackermann, *ACS Catal.*, 2020, **10**, 10551–10558.

23 J. Park, J. Lee and S. Chang, *Angew. Chem., Int. Ed.*, 2017, **56**, 4256–4260.

24 H. Shizuka, M. Serizawa, H. Kobayashi, K. Kameta, H. Sugiyama, T. Matsuura and I. Saito, *J. Am. Chem. Soc.*, 1988, **110**, 1726–1732.

25 (*a*) Y. L. Sun and A. T. Wu, *J. Fluoresc.*, 2013, **23**, 629–634; (*b*) Y. Tang, H. Liu, G. Jiang and Z. Gu, *J. Appl. Spectrosc.*, 2017, **84**, 911–914.

26 (*a*) Y. C. Hsieh, J. L. Chir, S. T. Yang, S. J. Chen, C. H. Hu and A. T. Wu, *Carbohydr. Res.*, 2011, **346**, 978–981; (*b*) N. Kaur, P. Kaur, G. Bhatia, K. Singh and J. Singh, *RSC Adv.*, 2016, **6**, 82810–82816; (*c*) S. Ta, S. Nandi, M. Ghosh, S. Banerjee and D. Das, *Spectrochim. Acta, Part A*, 2017, **173**, 196–200.

27 (*a*) B. D'Autréaux, N. P. Tucker, R. Dixon and S. Spiro, *Nature*, 2005, **437**, 769–772; (*b*) H. Weizman, O. Ardon, B. Mester,

J. Libman, O. Dwir, Y. Hadar, Y. Chen and A. Shanzer, *J. Am. Chem. Soc.*, 1996, **118**, 12368–12375; (*c*) D. S. Kalinowski and D. E. S. R Richardson, *Pharmacol. Rev.*, 2005, **57**, 547–583; (*d*) A. Gupta and A. L. Crumbliss, *J. Lab. Clin. Med.*, 2000, **136**, 371–378.

28 (*a*) S. Meghdadi, N. Khodaverdian, A. Amirnasr, P. J. French, M. E. van Royen, E. A. C. Wiemer and M. Amirnasr, *J. Photochem. Photobiol., A*, 2020, **389**, 112193; (*b*) X. Gong, H. Zhang, N. Jiang, L. Wang and G. Wang, *Microchem. J.*, 2019, **145**, 435–443.

29 A. Shylaja, S. R. Rubina, S. S. Roja and R. R. Kumar, *Dyes Pigm.*, 2020, **174**, 108062–108070.

30 S. Mohandoss, R. Atchudan, T. N. J. I Edison, K. Mishra, R. J. I. Tamargo, S. Palanisamy, K. Yelithao, S. G. You and Y. R. Lee, *Sens. Actuators, B*, 2020, **306**, 127581–127594.